# Inorganic profiles of preimplantation embryos reveal a role for zinc in blastocyst development

Julia L. Balough[1,2], Thomas V. O'Halloran[3‡], Francesca E. Duncan[2], Teresa K. Woodruff[4‡]

[1]Department of Obstetrics, Gynecology and Reproductive Sciences, University of Pittsburgh School of Medicine, Pittsburgh, Pennsylvania, USA

[2]Department of Obstetrics and Gynecology, Feinberg School of Medicine, Northwestern University, Chicago, Illinois, USA

[3]Department Microbiology, Genetics and Immunology and Department of Chemistry, Michigan State University, East Lansing, Michigan, USA

[4]Department of Obstetrics and Gynecology, Michigan State University, East Lansing, Michigan, USA

‡Correspondence:

Teresa K. Woodruff, PhD

Department of Obstetrics and Gynecology

Michigan State University

East Lansing MI 49719

Email: tkw@msu.edu

‡Thomas V. O'Halloran

Department Microbiology, Genetics and Immunology

Michigan State University

East Lansing MI 49719

Email: ohallor8@msu.edu

**Keywords:** Zinc, preimplantation embryo, embryo development, inner cell mass

**Word Count:** 4905

**Abstract**

Elements such as iron, copper and zinc play essential roles in the mammalian oocyte, egg, and embryo, however among these metals, zinc plays unique regulatory roles. Temporal fluctuations in zinc concentrations drive reproductive milestones such as meiotic resumption, egg activation, and initiation of the mitotic cell cycle. Roles for zinc in late preimplantation embryo development, have not been well characterized. Using a quantitative element approach we report the inorganic profiles of mouse embryos progressing through the late blastocyst stage. We find that blastocysts, like oocytes and eggs, and distinct to somatic cells, maintain higher levels of zinc than copper and iron. All three of these essential metals are more abundant in the inner cell mass, which contains the population of pluripotent stem cells that give rise to the fetus, relative to the trophectoderm which gives rise to the placenta and extraembryonic tissues. To test whether zinc abundance was associated with mitotic progress and cell fate lineage, we perturbed zinc homeostasis during blastocyst formation by artificially raising intracellular zinc concentrations with zinc pyrithione. This treatment during the morula-to-blastocyst transition when cell fate lineages emerge resulted in an elevation of zinc in the ICM. This treatment did not impact cell number, but did increase expression of the pluripotency and epiblast marker, *Nanog*, and decreased expression of the primitive endoderm marker, *Gata4*. These results demonstrate that the inorganic profiles of the late preimplantation embryo retain elemental hallmarks of earlier developmental stages and perturbation of zinc levels alters pluripotency gene expression in the blastocyst.

## Introduction

Transition metals, such as Mn, Fe, Co, Cu, Zn and Mo, play highly specific structural and catalytic roles that are necessary for proper cellular functioning (Eide, 2006, Uriu-Adams and Keen, 2010). Among these metals, zinc plays a variety of unique physiological roles in control of developmental processes. Highly localized fluctuations in zinc content drive regulatory events during maturation and activation of the female gamete. For instance, spatial-temporal fluctuations in zinc concentrations in the oocyte regulate the switch between meiotic arrest and resumption in the fertilized egg and the initiation of mitosis in the preimplantation embryo (Kim et al., 2010, Bernhardt et al., 2011, Kim et al., 2011, Bernhardt et al., 2012, Kong et al., 2012, Tian et al., 2014, Kong et al., 2015, Duncan et al., 2016, Zigo et al., 2022, Chen et al., 2023). These reproductive cell types have unique inorganic signatures relative to somatic cell types in that zinc is the most abundant transition metal, existing at an order of magnitude higher than other elements such as iron and copper (Kim et al., 2010, Kong et al., 2015).

A suite of single cell analysis methods, including synchrotron-based x-ray microscopy (XFM), as well as small molecule perturbations of metal content have been essential to establishing these roles for zinc. For example, the concentration of zinc increases by 50% during meiotic maturation, and this rise is essential for the oocyte to reach metaphase of meiosis II (MII). Preventing this zinc accrual with a zinc chelator, N,N,N′,N′-tetrakis-(2-pyridylmethyl)-ethylenediamine (TPEN), results in an arrest at a telophase I-like stage (Kim et al., 2010, Kim et al., 2011). In contrast to the increase of zinc that occurs during meiotic maturation, fertilization triggers a decrease via the exocytosis of 10 billion zinc atoms in what has been termed the “zinc spark” (Kim et al., 2011, Duncan et al., 2016). If the fertilized egg fails to release zinc at this stage or if zinc content is experimentally elevated using a zinc ionophore, zinc pyrithione (ZPT), eggs do not complete meiosis, fail to progress into mitosis, or begin to reform the metaphase II spindle and actin cap (Kim et al., 2011). Following fertilization, zinc levels remain relatively stable, and higher than both copper and iron, throughout 8-cell stage of

preimplantation embryo development (Kong et al., 2015). Chelation of zinc in cleavage stage embryos, specifically in 2- and 4-cell embryos, results in developmental arrest due to failed mitosis, altered chromatin structure, and inhibition of global transcription (Kong et al., 2015). These findings demonstrate an important function of zinc in early preimplantation embryo development, but its role in later stages, namely the morula and blastocyst stages, has not been systematically investigated.

There are multiple cellular events that occur during preimplantation embryo development, including the maternal-to-zygotic transition, compaction and polarization of internal and external cell populations, and cell lineage specification (Zernicka-Goetz et al., 2009, Jedrusik, 2015). The blastocyst is the result of the first cell fate decision in mammals. In the early cleavage embryo, the blastomeres are totipotent and have the potential to become all cell and tissue types; however, this potential is lost as the embryo develops through the 8-cell, morula and blastocyst (Suwinska et al., 2008, Maemura et al., 2021). The blastocyst contains two cell populations: the inner cell mass (ICM) which will give rise to all embryonic cell types and the trophectoderm (TE) cells which develop into extraembryonic cell types such as the placenta(Zernicka-Goetz et al., 2009). The ICM and TE cell populations are characterized by exclusive expression of several transcription factors. *Cdx2,* caudal type homeobox 2, is a gene specifically expressed in the TE that inhibits the pluripotency marker *Oct4*. *Oct4* (*Pou5f1)* is a POU-domain transcription factor highly expressed in the ICM. *Oct4* expression is necessary for induction of pluripotency and upregulates pluripotent maintenance factor, *Nanog,* while inhibiting expression of *Cdx2(Zernicka-Goetz et al., 2009, Wu et al., 2010).* The mechanisms of cell partitioning and cell fate determination in the preimplantation embryo are essential for blastocyst formation, implantation, and fetal development.

In this study, we defined the elemental content of that late preimplantation embryo utilizing synchrotron-based XFM and assessed the effect of elevated zinc during blastocyst development. We demonstrated that total zinc levels are constant from the 8-cell through

blastocyst stages, and that zinc content is significantly higher in each of these stages compared to iron and copper. Further we observed a striking enrichment of zinc atoms in the ICM of the blastocyst. To determine whether zinc homeostasis is important for blastocyst formation, we utilized zinc pyrithione (ZPT) treatment to elevate zinc content during the morula-to-blastocyst transition and evaluated its impact on blastocyst formation. We defined a minimal level of ZPT treatment that effectively increased zinc. While ZPT had no effect on total, ICM, or TE cell number in the resulting blastocysts, this treatment did induce an increase in pluripotency marker gene expression. These results support the importance of zinc homeostasis during late preimplantation embryo development and suggest a regulatory role in cell identity within the ICM.

## Materials and Methods

*Animals and breeding*

Female CD1 mice, aged 6-8 weeks, were obtained from Envigo (Madison, WI, USA) and housed in a controlled barrier facility at Northwestern University's Center for Comparative Medicine (Chicago, IL, USA). All animals were maintained in accordance with Northwestern University's Institutional Animal Care and Use Committee (IACUC). Humidity, temperature and photoperiod (14 light: 10 dark) were kept constant and food (Teklad Global irradiated chow 2916) and water were provided ad libitum. To maximize embryo yield, female mice were hyperstimulated by intraperitoneal injection of 10 IU pregnant mare's serum gonadotropin (PMSG, EMD Bioscience, San Diego, CA, USA). 44-46 hours later female mice were superovulated with 10 IU human chorionic gonadotropin (hCG, Sigma-Aldrich, St. Louis, MO, USA). Next, two female mice were paired with one male CD1 mouse (aged 10-25 weeks) for trio breeding.

*Embryo collection and preparation for X-ray fluorescent microscopy (XFM)*

Eight-cell, morula, and blastocysts were collected from mated females at 72, 96 and 120 hours post-hCG, respectively. The oviduct and uteri of bred female mice were collected into dissection media containing Leibovitz's L-15 medium (L-15, Sigma Aldrich, St. Louis, MO, USA) supplemented with 0.1% polyvinyl alcohol (PVA, Sigma Aldrich, St. Louis, MO, USA) and cut with scissors to release the embryos. Embryos were collected and washed in pre-equilibrated (37□C, 5% $CO_2$) potassium complex optimized media (KSOM, EMD Millipore, Burlington, MA, USA). Early blastocysts were characterized by a blastocoel cavity <50% of total embryo volume and late blastocysts had blastocoels >50% total embryo volume. Embryos were prepared for XFM as previously described(Kim et al., 2010, Kong et al., 2015). Briefly, embryos were washed three times in 100 mM, pH 7 ammonium acetate to remove metal salts. Next embryos were loaded on a 2 mm x 2 mm silicon nitride window (Norcada Inc., Canada), excess media was removed by wicking and embryos air dried and were stored at room temperature until imaging.

*X-ray fluorescence imaging and quantification*

XFM was performed at the Advanced Photon Source on beamline 2-ID-E at the Argonne National Laboratory as previously described(Kong et al., 2015). In brief, 10 keV X-rays were monochromatized and focused to a spot size of 0.5 μm x 0.5 μm using Fresnel zone plate optics. Raster scans were done using fly-scan mode with a 0.5-μm step size and a dwell time of 50 ms. Fluorescence spectra were collected using a silicone drift detector (Vortex-ME4). Fluorescence spectra were integrated along the z-axis, calibrated using thin film standard from AXO (AXO DRESDEN, Dresden, Germany) and two-dimensional elemental maps were built for each element to display elemental concentration in units of $\mu g/cm^2$. Image processing and analysis were performed using MAPS 1.8.0.00 software and the elemental content was determined for specific regions of interest (ROI) that were established using the phosphorus channel; ROIs included: whole embryo, ICM and TE, as well as background which was subtracted after normalization for area(Chen et al., 2023).

*Zinc pyrithione treatment*

Previous studies have shown egg cytotoxicity upon treatment with ZPT (Sigma-Aldrich, St. Louis, MO, USA) concentrations of 10, 20 or 50 µM sometimes with 5-10 minute treatment window(Taki et al., 2004, Kim et al., 2011, Bernhardt et al., 2012). To establish an optimal concentration of ZPT that increased intracellular zinc but did not induce toxicity, a 10-1000 nM dose response embryo culture assay was performed. A 50 µM stock solution of ZPT in dimethyl sulfoxide (DMSO, Sigma-Aldrich, St. Louis, MO, USA) was made and diluted as described below. Female mice were hyperstimulated, superovulated and mated as previously described. 36 hours after pairing for trio breeding, two-cell embryos were collected from the oviducts of mated females into Leibovitz's L-15 medium (L-15, Sigma Aldrich, St. Louis, MO, USA) supplemented with 0.1% polyvinyl alcohol (PVA, Sigma Aldrich, St. Louis, MO, USA). Any unfertilized, fragmented or unsynchronized embryos were discarded. Two-cell embryos were cultured for 48 hours in Advanced KSOM (EMD Millipore, Billerica, MA, USA) in an incubator (37□C, 5% $CO_2$) until the morula stage. Because the treatment time was increased to 24 hours to capture morula to blastocyst transitions, the dose response assay was performed with ZPT at concentrations of 0 nM (vehicle control), 10 nM, 100 nM and 1 µM. Morulae were cultured in KSOM with control or ZPT for 24 hours and assessed for blastocyst development. Live embryos were imaged on brightfield on EVOS FL Auto Cell Imaging System (Thermo Fisher Scientific, Waltham, MA) at 10X. The maximum concentration that showed no statistical difference in embryo development was 100 nM ZPT and was used for all subsequent experiments.

*Labile zinc labeling and live-cell imaging*

To assess if ZPT treatment led to an increase in intracellular zinc content, labile zinc concentration was evaluated after treating live embryos with the vital zinc-responsive fluorescent probe ZincBY-1(Que et al., 2015). Vehicle or ZPT treated blastocysts were

incubated for 30 minutes prior to imaging with 50 nM ZincBY-1, a labile zinc-specific fluorophore, and 1 μg/ml Hoescht 33342 (Thermo Fisher Scientific). Blastocysts were rinsed and loaded into pre-equilibrated KSOM drops under mineral oil (Irvine Scientific, Santa Ana, CA, USA) on a glass bottom dish (MatTek Corporation, Ashland, MA, USA). Confocal microscopy was performed on a Leica TCS SP5 inverted laser-scanning confocal microscope (Leica Microsystems, Heidelberg, Germany) at 10X air objective. All exposure and microscope settings including laser power, gain, pinhole and zoom were set to the ZPT treatment group and kept constant for all embryos. Z-stacks were taken of each embryo with a step size of 1AU. Image analysis for signal intensity was performed in ImageJ (NIH, Bethesda, MD, USA). Z-stack image files were compressed into a single maximum projection image. Using the threshold tool, maximum and minimum threshold for each embryo were selected and total intensity was measured. Absolute intensity for each embryo was determined by dividing the area of the embryo from the raw intensity density.

*Quantitative real-time PCR*

Sets of 50 blastocysts per control or treatment group were isolated and lysed in 50 μl of extraction buffer from the Arcturus PicoPure RNA Isolation Kit (Thermo Fisher Scientific) and snap frozen and stored at -80ºC until RNA isolation. RNA isolation was performed per manufacturers recommendations with on-column DNase I treatment. Eluted RNA was reverse transcribed, and cDNA was synthesized using SuperScript III First-Strand cDNA synthesis kit with random hexamers (Thermo Fisher Scientific). Real time PCR was performed using SYBR green master mix and primers (Supplemental Table 1) (Integrated DNA Technologies) on the StepOnePlus real time PCR system (Applied Biosystem) with 56ºC annealing temperature and 40 run cycles. Each PCR plate run included 3 internal replicates per treatment and gene. Changes in expression were expressed as fold change using the $2^{-\Delta\Delta Ct}$ method and normalized to *B-actin* expression.

*Blastocyst immunocytochemistry*

Blastocysts were fixed in 3.8% paraformaldehyde for 1 hour then washed through blocking buffer (PBS containing 0.3% BSA, 0.01% Tween-20 and 0.02% $NaN_{3)}$. Blastocysts were permeabilized in 1X PBS, 0.3% BSA, 0.1% Triton X-100, and 0.02% $NaN_3$ for 20 minutes then washed through blocking buffer. Embryos were incubated overnight at 4□C in mouse monoclonal anti-CDX2 (1:100, BioGenex, MU392A) and rhodamine phalloidin (1:200, Thermo Fisher Scientific, R415). Embryos were washed through blocking buffer and incubated in Alexa Fluor-488 donkey anti-mouse IgG (1:200, Invitrogen, A21202) secondary antibody for 1 hour at 37□C. Embryos were washed through blocking buffer and moved through a Vectashield+DAPI gradient (25%, 50%, 75% in blocking buffer) then mounted in 100% Vectashield+DAPI (H-1200, Vector Laboratories, Inc.). Images were taken using a Leica TCS SP5 inverted laser-scanning confocal microscope (Leica Microsystems) at 40X oil immersion objective. Z-stacks were taken of 1AU section thickness. Images were processed using ImageJ (NIH, Bethesda, MD, USA). For cell counting, newly appearing nuclei were annotated on each stack of the total z-stack. Total embryo cells were determined with DAPI, TE cells were CDX2+ nuclei and ICM were CDX2- nuclei. Mitotic cells were determined by counting cells in metaphase or anaphase per total cells counted.

*RNAscope*

RNAscope was performed according to manufactures instructions using the RNAscope Multiplex Fluorescent v2 Assay and protocol as previously described(Xie et al., 2018). In brief, blastocysts were fixed in 100 µl of 3.8% paraformaldehyde and 0.1% polyvinylpyrrolidone overnight. To detect TE and ICM transcripts, probes synthesized against the mouse *Cdx2* (438921), *Pou5f1(Oct4)* (426961), *Nanog* (501891) and *Gata4* (417881) were used (Advanced Cell Diagnostics). All reagents were provided with the RNAscope Multiplex Fluorescent v2

Assay. Opal fluorophores 520. 570, 690 (Akoya Biosciences, Marlborough, MA) were used as secondary antibodies. Embryos were imaged on the Leica TCS SP5 inverted laser-scanning confocal microscope (Leica Microsystems) at 40X oil immersion objective. Z-stacks were taken of 1AU section thickness. Transcripts per embryos were captured by measuring intensity using ImageJ (NIH, Bethesda, MD, USA). Transcript intensity for each embryo was determined by dividing the area of the embryo from the raw intensity density of the transcript.

*Statistical analysis*

Data analysis was performed using Graphpad Prism 9 software. Data was tested for normal distribution with the Shapiro- Wilk test. When appropriate multiple comparisons were tested with one-way ANOVA or Kruskal-Wallis ANOVA. For a single comparison, unpaired t-test or Mann-Whitney test was used. Values are expressed in mean ± standard deviation unless otherwise stated. A P-value <0.05 was considered significant.

## Results

*Iron, copper and zinc content across the late preimplantation embryo*

To determine the elemental composition of zinc, iron, and copper throughout late preimplantation embryo development, we performed synchrotron-based XFM on 8-cell, morula, early and late blastocysts derived from *in vivo* matings (Fig. 1A, Supp. Figs. 1-4). Similar to the oocyte, egg, and cleavage stage embryo, zinc is the most abundant transition metal compared to iron and copper on average across the 8-cell, morula, and blastocyst (Table 1)(Kim et al., 2010, Kong et al., 2015). While previous studies show increasing copper and zinc content during meiotic maturation in the oocyte, the total number of copper and zinc atoms in the embryo remained constant through late preimplantation embryo development (Table 1 and Fig. 1B)(Kim et al., 2010, Kong et al., 2015). Interestingly, we observed an increase in iron atoms at the 8-cell stage which remained high through the morula and early blastocyst stages and

decreased in the late blastocyst (Fig 1B, $p<0.05$)(Kong et al., 2015). To illustrate the abundance of zinc atoms in the late preimplantation embryo, we compared the ratio of zinc atoms to copper and iron. There was a 16-23 fold increase in zinc atoms compared to copper atoms across all stages (Table 1). When comparing the ratio of total zinc atoms to iron atoms, we observed approximately 2-fold increase in atom abundance of zinc at the 8-cell, morula and early blastocyst which doubled to over a 4-fold difference in Zn to Fe atoms in the late blastocyst (Table 1, Fig. 1C, $p<0.05$).

*Zinc is enriched in the ICM of the blastocyst*

Because of the striking localization of zinc atoms in the inner cell mass of the late blastocyst (Fig. 1A), we performed a more in-depth analysis of the XFM data based on defined regions of interest (Fig. 2A). We confirmed that total zinc in the late blastocyst is significantly higher than both iron and copper (Table 1, Fig. 2B, $p<0.001$). Using the phosphorous maps to define regions of interest that had high cell density in the blastocyst, we estimated the metal content of the TE and ICM. In general, we observed the number of iron, copper and zinc atoms per $\mu m^2$ in the ICM ($1.72 \times 10^6$, $4.07 \times 10^5$, $7.82 \times 10^6$) was higher compared to the TE ($9.38 \times 10^5$, $2.97 \times 10^5$, $3.86 \times 10^6$ atoms/$\mu m^2$)(Fig. 2C, $p<0.001$). The ratio of ICM to TE metal atoms per area was significantly increased in iron (1.9) and zinc (2.1) compared to copper (1.4) (Fig 2D, $p<0.05$). Taken together, we observed that zinc is the most abundant transition metal in the blastocyst compared to iron and copper with more than double the concentration of zinc atoms in the ICM.

*Zinc homeostasis is required for the morula-to-blastocyst transition*

Given that zinc is the most abundant transition metal in the late blastocyst and displays an accumulation in the ICM, which is the site of pluripotent stem cells, we sought to determine the functional significance of zinc fluctuations during the late stages of embryo development.

Zinc availability can be limited in biological samples through treatment with intracellular chelators or increased by treatment with zinc ionophores. We have previously shown that zinc availability is essential for mitosis in the cleavage stage embryo, since chelation using TPEN blocks cell cycle progression and precludes development (Kong et al., 2015). Therefore, to determine the role of zinc during the morula-to-blastocyst transition, we perturbed zinc homeostasis in the murine embryo using a model of zinc excess where ZPT was used to elevate intracellular zinc (Fig. 3A)(Taki et al., 2004, Kim et al., 2011, Bernhardt et al., 2012). We first performed a dose-response assay to determine the maximal dose of ZPT that increased zinc without impacting the morula-to-blastocyst transition. To do this, morulae were cultured in control (0 nM), 10 nM, 100 nM and 1 μM of ZPT for 24 hours, and the number of blastocysts or degenerating embryos was scored (Fig. 3B). There was no effect on blastocyst development with 10 nM (83.3 ± 11.6%) or 100 nM (76.7 ± 11.6%) ZPT compared to control (83.3 ± 5.8%) ($p>0.05$). However, treatment with 1 μM ZPT led to the development of significantly fewer blastocysts (23.3 ± 20.8%) compared to the other doses (Fig. 3C, $p<0.05$). These results demonstrate embryos readily tolerate as much as 100 nM ZPT during the morula to blastocyst transition; however, ZPT treatment of 1 μM is toxic and impairs blastocyst development.

*ZPT treatment increases intracellular labile zinc content*

While 1 μM of ZPT was cytotoxic to embryos, 100 nM of ZPT did not perturb blastocyst development. To determine whether 100 nM ZPT treatment led to elevation of intracellular zinc levels in treated embryos, we performed live staining with a labile zinc probe, ZincBY-1(Que et al., 2015). After morulae were cultured for 24 hours in control (0 nM) or 100 nM ZPT and developed into blastocysts, they were then incubated for 30 minutes with ZincBY-1 to visualize labile zinc and Hoescht (Fig. 3D). Live blastocysts were imaged with the same exposure settings and the intensity of ZincBY-1 signal was measured. The intensity of ZincBY-1 signal was higher in the ZPT treated blastocysts ($5.77 \times 10^4 \pm 3.21 \times 10^4$) compared to controls (3.48 x

$10^4$ ± 2.21 x $10^4$ raw intensity/area) (Fig. 3E, $p<0.05$). These findings indicate that ZPT treatment effectively increased intracellular zinc content.

*The zinc transporter network is altered with ZPT treatment*

We next assessed whether ZPT treatment during the morula-to-blastocyst transition impacted expression of genes that regulate zinc into and out of cells. We performed RT-qPCR on control or treated blastocysts and analyzed the gene expression of zinc importers (ZIPs), *Slc39a* genes, or zinc exporters (ZNTs), *Slc30a* genes. The ZIP family increases cytosolic zinc by transporting zinc into the cytosol from the extracellular compartment or from intracellular vesicles, whereas the ZNT family reduces cytosolic zinc levels by promoting efflux into the extracellular regions or influx into vesicles (Liuzzi and Cousins, 2004). ZPT treatment at 100nM did not change the expression of the majority of the zinc transport network. However, there was a decrease in *Slc39a13 (Zip13*) expression (0.58 ± 0.19) and a robust increase in *Slc30a9 (Znt9)* expression (6.83 ± 0.38-fold change to control) (Fig. 3F and G, $p<0.05$). *Zip13* is a zinc importer located in multiple cellular compartments including the endoplasmic reticulum, Golgi apparatus, and cytosolic vesicles (Takagishi et al., 2017). Similarly, *Znt9,* a zinc exporter, is localized to mitochondria and regulates zinc homeostasis(Deng et al., 2021, Kowalczyk et al., 2021). These results demonstrate a functional response to zinc perturbation.

*Excess zinc does not impair mitosis in the blastocyst*

Given that zinc is an essential cofactor for mitosis and is necessary to support embryo development, we tested whether increasing intracellular zinc during the morula-to-blastocyst transition impacts the number of resulting blastocysts. Blastocyst cell number is indicative of developmental outcomes and implantation success (Lane and Gardner, 1997, Kong et al., 2016, Guzman et al., 2019). To assess blastocyst cell number, we stained blastocysts with Hoechst to count total nuclei (Fig. 4A). There was no difference in total nuclei in control (91.7 ± 20.6) or

treated blastocysts (87.7 ± 19.8 nuclei per embryo) (Fig. 4B, $p>0.05$). By performing immunofluorescence with an antibody for CDX2, a marker for the TE lineage, we next tested whether there was a difference in the fraction of TE or ICM cells after ZPT treatment. For trophectoderm cells, there were 0.81 ± 0.11 CDX2 positive nuclei/total nuclei in control embryos and 0.78 ± 0.07 CDX2+ nuclei/total nuclei in ZPT treated embryos (Fig. 4C, $p>0.05$). CDX2 negative nuclei were counted as a proxy for ICM cells, and there was no difference between control (0.19 ± 0.11) and ZPT treated blastocysts (0.22 ± 0.07 CDX2- nuclei/total nuclei)(Fig. 4D, $p>0.05$). Thus, elevated zinc during blastocyst development did not impact total numbers of TE or ICM cells. Next, we assessed whether ZPT treatment impacted the mitotic index or the number of cells that were in metaphase or anaphase. There was no difference in the mitotic index between control (0.03 ± 0.02) and treated (0.04 ± 0.03 mitotic/total cells) blastocysts (Fig. 4E, $p>0.05$). Lastly to confirm the number of mitotic cells was equivalent in these embryos, we assessed if there was a difference in the ratio of CDX2 positive and negative mitotic cells and found the ratio was the same in control and treated embryos (Fig. 4F, $p>0.05$). Here, we demonstrate that elevated levels of intracellular zinc does not alter the number of cells in the resulting blastocyst.

*Zinc ionophore treatment during the morula to blastocyst transition alters expression of pluripotency gene, Nanog, and primitive endoderm gene, Gata4*

Given that the number of TE and ICM cells was similar in the blastocyst with excess zinc, we next tested whether zinc elevation altered expression of key genes involved in maintaining pluripotency in the ICM and TE lineage using RT-qPCR. There was no difference in the fold change expression of *Oct4* (1.58 ± 0.98) and *Sox2* (0.94 ± 0.20) in ZPT treated embryos relative to control embryos (Fig. 5A, $p>0.05$). However, we did observe an increase in *Nanog* (1.35 ± 0.15) expression and a decrease in *Gata4* (0.81 ± 0.11 fold change) expression compared to control (Fig. 5A, $p<0.05$). Although both *Nanog* and *Gata4* are expressed in the

ICM of the blastocyst, *Nanog* is a key factor in maintaining pluripotency and the epiblast lineage whereas *Gata4* is a differentiation marker that gives rise to the primitive endoderm(Mitsui et al., 2003, Rojas et al., 2010). Genes involved in the TE lineage were unaffected by zinc, as there was no significant fold change in expression for *Cdx2* (0.99 ± 0.23), *Eomes* (0.94 ± 0.15), or *Tead4* (1.3 ± 0.47-fold change) compared to control (Fig. 5B, $p>0.05$). While RT-qPCR was performed on bulk control and treated blastocysts, we performed orthogonal validation using RNAscope of cell fate genes in whole-mount blastocysts (Fig. 5C, D, E). This method of fluorescent in situ hybridization allows for visualization of single RNA transcripts, and we used fluorescent intensity to quantify transcript abundance. Consistent with our qPCR data, we observed no difference in *Cdx2* transcript ($4.12 \times 10^4 \pm 2.45 \times 10^4$ and $3.13 \times 10^4 \pm 1.62 \times 10^4$) or *Oct4* transcript ($4.14 \times 10^4 \pm 2.14 \times 10^4$ and $2.75 \times 10^4 \pm 1.72 \times 10^4$ raw intensity of transcript/area) abundance between treated and control embryos (Fig. 5F, G, $p>0.05$). The increase in *Nanog* transcript abundance with ZPT treatment ($1.91 \times 10^4 \pm 3.88 \times 10^3$) compared to control ($1.12 \times 10^4 \pm 4.54 \times 10^3$ raw intensity/area) was also consistent with the qPCR results (Fig. 5H, $p<0.05$). However, no difference was observed in the abundance of *Gata4* transcripts between control ($1.91 \times 10^4 \pm 6.33 \times 10^4$) and treated blastocysts ($1.83 \times 10^4 \pm 4.82 \times 10^4$ raw intensity/area) (Fig. 5I. $p>0.05$). Taken together we observed that elevated zinc during the morula-to-blastocyst transition enhanced expression and abundance of the pluripotency marker, *Nanog,* in blastocyst.

## Discussion

The developmental capacity of the preimplantation embryo is based on the quality of the female gamete. Zinc is an essential factor in female gamete quality as zinc accumulation is needed for oocyte meiotic maturation, and zinc release occurs at fertilization and is essential for egg activation and initiating the mitotic cell cycle(Kim et al., 2010, Bernhardt et al., 2011, Kim et al., 2011, Bernhardt et al., 2012, Kong et al., 2012, Tian et al., 2014, Kong et al., 2015, Duncan

et al., 2016, Chen et al., 2023). In this study we expanded the growing body of work highlighting zinc as an essential factor in reproduction and development by defining the role of zinc as the preimplantation embryo progresses from the morula to the blastocyst stage. Blastocyst development is imperative as it is the stage when extra-embryonic tissues that support pregnancy are differentiated from the cells that develop into fetal tissue types. Specifically in the late blastocyst, the number of zinc atoms are 16 times greater compared to copper and 4 times greater than iron. To determine whether zinc regulates cell fate determination, we utilized a model of zinc excess at levels that were not cytotoxic. ZPT treatment at 100 nM increased intracellular zinc without compromising progression to the blastocyst stage. Although blastocyst number was not impacted, excess zinc enhanced *Nanog* expression and transcript abundance in the blastocyst. These results highlight zinc as a potential cofactor for pluripotency regulation in the developing embryo.

Small molecules that perturb zinc availability are key tools in our arsenal to for evaluation of zinc roles during development. The chelating agent TPEN has been useful in establishing that elevated levels of zinc in the oocyte are required to maintain cell cycle arrest, prohibit meiotic resumption and control cytoplasmic division during polar body extrusion(Kim et al., 2010, Bernhardt et al., 2012). In the egg, TPEN-chelation of zinc can mimic the 20% reduction in total zinc levels that occurs at fertilization and initiate the final stages of egg activation(Kong et al., 2012). TPEN-chelation of zinc at the 2- or 4- cell embryo arrests the embryo by initiating quiescent global transcription (Kong et al., 2015). Because zinc is a critical cofactor for mitosis, similar chelation studies cannot be used as easily to investigate zinc homeostasis in the late stage preimplantation embryo. Therefore, we utilized an agent that elevated intracellular zinc to perturb zinc homeostasis. While oocytes can withstand 10 μM in ZPT treatment with no cytotoxicity, we saw significant reductions in development when morulae were treated with 1 μM ZPT. Through dose response studies we established a working concentration of ZPT (100 nM) that was high enough to elevate intracellular zinc availability but

not induce toxicity (Kim et al., 2011). mRNA levels of the *Slc39a13* zinc importer (*Zip13*) were decreased and the *Slc30a9* zinc exporter (*Znt9*) were elevated following ZPT treatment, demonstrating embryo responsiveness to elevations in intracellular zinc. The embryo appears more sensitive to perturbations that elevate zinc availability than oocytes. This difference may arises from the known transcriptional quiescence in the fully grown oocyte compared to the later stage preimplantation embryo where zinc can act as an enzymatic cofactor, a secondary messenger, and a transcription factor (Chen et al., 2024).

XFM revealed a two-dimensional representation of metal content and a striking accumulation of zinc in the ICM of the blastocyst. Elevating zinc during the morula-to-blastocyst transition, when cell fate lineages emerge, resulted in an increased expression of pluripotency and epiblast marker, *Nanog*, and a slight decrease in expression of the primitive endoderm marker, *Gata4*. These results along with the visual accumulation of zinc in the ICM suggest an association of zinc level with pluripotency in the intact blastocyst. Indeed, studies of murine embryonic stem cells treated with zinc chloride also show an increase in *Nanog* expression and a decrease in *Gata4* supporting our results that zinc content may play a regulatory role in cell fate (Hu et al., 2016). Further, zinc is emerging as an alternate media factor to maintain pluripotency in embryonic stem cell culture. In feeder free conditions with media supplemented with zinc, embryonic stem cell maintained self-renewal with gene expression profiles of *Oct4, Nanog* and *Klf4* similar to the traditional Leukemia inhibitory factor (LIF) supplemented media (Mnatsakanyan et al., 2019). The mechanism of zinc regulation of embryonic stem cell reprogramming is still under investigation; however, several zinc finger proteins, *Zfp143* and *Zfp281*, are transcription factors that interact with the promoter region of *Nanog* to modulate stem cell self-renewal or differentiation (Chen et al., 2008, Kim et al., 2008, Wang et al., 2008, Fidalgo et al., 2011). Thus, the body of work is growing in support of zinc as a co-factor for cell fate programming in embryonic stem cells.

In contrast to copper and zinc levels which remain relatively stable through the late embryo, iron levels increased at the eight-cell, morula and early blastocyst and significantly decreased in the late blastocyst. An increase at the eight-cell stage was previously observed and hypothesized to be due to an initiation of mitochondrial respiration and glucose utilization at the blastocyst (Houghton and Leese, 2004, Kong et al., 2015). However, our results suggest this signature is lost at the late-blastocyst stage. Like zinc, iron homeostasis during development is necessary for metabolism, oogenesis, embryo development and reproductive outcomes(Sieber et al., 2016, Ng et al., 2019, Fisher et al., 2021). Iron excess during embryo development results in impaired blastocyst formation with increased apoptotic and ferroptosis rates which was rescued with iron chelation (Chen et al., 2021). The proposed mechanism of dysfunction was also linked to the mitochondria as iron excess induced loss of mitochondrial membrane potential and ATP generation (Chen et al., 2021). These descriptive studies suggest that alterations in iron content may be involved in proper mitochondrial function as the embryo transitions from cleavage to early blastocyst and further investigation of iron homeostasis is the embryo is warranted.

The results from our study expand our understanding of inorganic physiology during mammalian development specifically during blastocyst development. We highlight the necessity for zinc during mitosis in the preimplantation embryo and contribute to the growing evidence that zinc content may support pluripotent cell identity.

**Acknowledgements**

This study used resources of the Advanced Photon Source, a U.S. Department of Energy (DOE) Office of Science User Facility, operated for the DOE Office of Science by the Argonne National Laboratory under contract no. DE-AC02-06CH11357. We would like to thank Northwestern University's Feinberg School of Medicine and Master of Reproductive Science and Medicine program for support, resources and expertise needed to bring together this team

and execute the study. We would like to thank Dr. Olga Antipova at the Argonne National Laboratory for assistance in acquiring and analyzing the XFM data, and Dr. Andrew Crawford for helpful discussions. We also thank Dr. Yuying Chen and Dr. Andrew Nowakowski for their contributions and resources in experimental planning and execution. Schematic (Fig. 3A) made using Biorender.

**Author Contributions**

J.L.B. wrote the proposal and performed the XFM at the Advanced Photon Source, designed and performed the mouse and *in vitro* experiments, analyzed the data, generated the figures and wrote the manuscript. T.V.O. was responsible for contributing to XFM data acquisition and analysis, utilization of the ZincBY-1 probe, and drafting of the manuscript. F.E.D. contributed to experimental design, data analysis and drafting of the manuscript. T.K.W. was responsible for conceiving, drafting and revising the manuscript and handling correspondence.

**Conflict of Interest**

The authors have no conflicts of interest to declare.

**Funding**

This work was supported by the Watkins Endowment (T.K.W.), NIGMS R01GM115848 (T.K.W., T.V.O.) and NIGMS P41GM135018 (T.V.O.).

## Figure Legends

*Figure 1. Synchrotron-based X-ray fluorescence microscopy illustrates elemental content of iron, copper and zinc through late preimplantation embryo development.*

A) Representative whole-mount eight-cell (8C, n=7), morula (M, n=6), early blastocyst (EB, n=10), and late blastocyst (LB, n=12) stage embryos used for XFM. Brightfield images after air-drying and corresponding elemental maps for iron (Fe), copper (Cu) and zinc (Zn) for each stage. Maps for Fe and Zn are shown at 0.00-0.20 and Cu is shown at 0.00-0.05 $\mu g/cm^2$ range. White areas on the elemental maps denote higher atom abundance. B) The mean ± SEM of total atoms per embryo for Fe, Cu and Zn. Kruskal-Wallis ANOVA, * $p<0.05$, ** $p<0.01$. C) The mean ± SEM ratio of total atoms between Zn and Fe across all embryo stages. Kruskal-Wallis ANOVA, * $p<0.05$, *** $p<0.001$

*Figure 2. XFM analysis of atoms in the trophectoderm (TE) and inner cell mass (ICM) regions of the late blastocyst*.

A) Representative brightfield and elemental maps for Fe, Cu and Zn in the late blastocyst. Inset shows phosphorus (P) map (0.00-25.0 $\mu g/cm^2$) which was used to define regions by cell density. TE region denoted in purple and ICM in blue. Maps for Fe and Zn are shown at 0.00-0.20 and Cu is shown at 0.00-0.05 $\mu g/cm^2$ range. B) Total atoms ± SD of Fe, Cu and Zn in the late blastocyst (n=12). Ordinary one-way ANOVA *** $p<0.001$, **** $p<0.0001$. C) The atoms per $\mu m^2$ of Fe, Cu and Zn in the TE (purple) and ICM (blue) (n=12 late blastocysts). Paired t-test, *** $p<0.001$, **** $p<0.0001$. D) The ratio of atoms per $\mu m^2$ in the ICM to the TE for Fe, Cu and Zn (n=12 late blastocysts). Ordinary one-way ANOVA, * $p<0.05$, ** $p<0.01$.

*Figure 3. Zinc ionophore, zinc pyrithione (ZPT), treatment during the morula-to-blastocyst transition.*

A) Experimental paradigm illustrating hyperstimulation and superovulation in CD1 female mice at 6-8 weeks old. Mice were mated and 2-cell embryos were collected and cultured *in vitro* until the morula stage. ZPT treatment was performed at the morula stage and after 24 hours blastocysts were collected for endpoint analysis. Schematic made in Biorender. B) Representative brightfield images of blastocysts cultured after 24 hours in control (0 nM), 10 nM, 100 nM and 1 μM ZPT. Insets display a healthy blastocyst or degenerating embryo. B) The percent (mean ± SD) of blastocysts developed from morulae cultured in ZPT for 24 hours. Each datapoint represents the average from a single trial of 10 embryos each. Ordinary one-way ANOVA, **$p<0.01$. C) Representative images of live blastocysts after ZincBY-1 staining. ZincBY-1 (green) stains labile since and Hoescht (blue) stains nuclei. Images are maximum projections of the z-stack. D) ZincBY-1 signal intensity (mean ± SD) of control (n=22) or ZPT treated (n=29) blastocysts. Mann-Whitney test, **$p<0.01$. E) Gene expression of zinc importers, the *Slc39a* family. Data is expressed as fold change (mean ± SD) in expression compared to control. One trial of 50 blastocysts per control and treated were used. Each datapoint represents an internal replicate. Data normalized to *B-actin* expression. Each gene was assessed by unpaired T-test, *$p<0.05$. F) Gene expression of zinc exporters, the *Slc30a* family. Data is expressed as fold change (mean ± SD) in expression compared to control. One trial of 50 blastocysts per control and treated were used. Each datapoint represents an internal replicate. Data normalized to *B-actin* expression. Each gene was assessed by unpaired T-test, ****$p<0.0001$. *Slc39a5, Slc39a8, Slc39a11, Slc39a12, Slc30a8,* and *Slc30a10* were included in the experiment but had no expression and are not shown.

*Figure 4. Mitotic endpoints in blastocysts treated with ZPT.*

A) Representative whole-mount blastocysts of control or ZPT treated blastocysts after immunocytochemistry for CDX2. Mid-sections of blastocysts stained with anti-CDX2 (red), rhodamine phalloidin (green), and DAPI (blue). Insets shows max projection of the z stack. B)

The total cells per embryo (mean ± SD) were determined by counting DAPI-nuclei in control (n=9) and treated blastocysts (n=10). Unpaired t-test, p>0.05. C) The number of CDX2+ nuclei per total nuclei (mean ± SD) determined the TE cells in the embryo (n=9/cohort). Unpaired t-test, p>0.05. D) The number of CDX2- nuclei per total nuclei (mean ± SD) determined the ICM cells in the embryo (n=9/cohort). Unpaired t-test, p>0.05. E) The mitotic index (mean ± SD) captures the cells in metaphase or anaphase of mitosis per total cells per embryo (n=9/cohort). Unpaired t-test, p>0.05. F) The ratio of mitotic cells(mean ± SD) that are CDX2+ (TE) or CDX2- (ICM) in control (n=9) and ZPT (n=7).

*Figure 5. Gene expression of cell fate markers in control and ZPT treated blastocysts.*

A) Gene expression of inner cell mass genes: *Oct4 (Pouf51), Nanog, Sox2* and *Gata4*. Data is expressed as fold change (mean ± SD) in expression compared to control. Each datapoint represents a trial of 50 blastocysts per control and treated groups. Three internal replicates were run per trial and averaged. Data normalized to *B-actin* expression. Each gene was assessed by unpaired T-test, ***p<0.001. B) Gene expression of trophectoderm genes: *Cdx2, Eomes,* and *Tead4*. Data is expressed as fold change (mean ± SD) in expression compared to control. Each datapoint represents a trial of 50 blastocysts per control and treated groups. Three internal replicates were run per trial and averaged. Data normalized to *B-actin* expression. Each gene was assessed by unpaired T-test, p>0.05. C) Representative mid sections of whole mount blastocysts after fluorescent in situ hybridization for *Cdx2* (red) and *Oct4* (green) transcripts. Each dot represents a single transcript. Inset displays max projection of z stack. DAPI (blue) stains nuclei. D) Representative mid sections of whole mount blastocysts after fluorescent in situ hybridization for *Cdx2* (red) and *Nanog* (green) transcripts. E) Representative mid sections of whole mount blastocysts after fluorescent in situ hybridization for *Cdx2* (red) and *Gata4* (green) transcripts. F) Transcript intensity per area (mean ± SD) for *Cdx2* per embryo (n=32 embryos/cohort). Unpaired t test, p>0.05. G) Transcript intensity per area (mean ± SD) for *Oct4*

per embryo (n=14 control and 12 ZPT treated embryos). Unpaired t test, $p>0.05$. H) Transcript intensity per area (mean ± SD) for *Nanog* per embryo (n=5 control and 11 ZPT treated embryos). Unpaired t-test, $^{**}p<0.01$. I) Transcript intensity per area (mean ± SD) for *Gata4* per embryo (n=14 control and 9 ZPT treated embryos). Unpaired t test, $p>0.05$.

*Table 1. Summary of numerical values for total iron, copper, and zinc in the preimplantation embryo by synchrotron-based-x-ray fluorescence microscopy*

*Supplemental Figure 1. Elemental Maps for Fe, Cu and Zn in the 8-cell embryo (n=7).*

Fe and Zn maps are shown at a minimum of 0.00 and maximum of 0.20 μg/cm$^2$ range. Cu maps are shown at 0.00-0.05 μg/cm$^2$. Whiter areas on the elemental maps denote higher atom abundance.

*Supplemental Figure 2. Elemental Maps for Fe, Cu and Zn in the morula(n=6).*

Fe and Zn maps are shown at a minimum of 0.00 and maximum of 0.20 μg/cm$^2$ range. Cu maps are shown at 0.00-0.05 μg/cm$^2$. Whiter areas on the elemental maps denote higher atom abundance. * denotes artifact that was excluded from analysis.

*Supplemental Figure 3. Elemental Maps for Fe, Cu and Zn in the early blastocyst (n=10).*

Early blastocysts were characterized by a blastocoel cavity <50% of embryo area. Fe and Zn maps are shown at a minimum of 0.00 and maximum of 0.20 μg/cm$^2$ range. Cu maps are shown at 0.00-0.05 μg/cm$^2$. Whiter areas on the elemental maps denote higher atom abundance.

*Supplemental Figure 4. Elemental Maps for Fe, Cu and Zn in the late blastocyst (n=12).*

Late blastocysts were characterized by a blastocoel cavity >50% of embryo area. Fe and Zn maps are shown at a minimum of 0.00 and maximum of 0.20 μg/cm$^2$ range. Cu maps are shown at 0.00-0.05 μg/cm$^2$. Whiter areas on the elemental maps denote higher atom abundance.

*Supplemental Table 1. Primers used for RT-qPCR*

**Table 1. Summary of numerical values for total iron, copper, and zinc in the preimplantation embryo by synchrotron-based-x-ray fluorescence microscopy**

| | Fe | Cu | Zn | Units | Zn:Fe (Ratio of Atoms) |
|---|---|---|---|---|---|
| Eight-cell | **17.6 ± 1.9** | **1.65 ± 0.2** | **35.3 ± 1.6** | Atoms x $10^9$ | 2.2 ± 0.2 |
| | *29.1 ± 2.6* | *2.74 ± 0.3* | *58.6 ± 2.5* | Atoms x $10^5/\mu m^2$ | |
| Morula | **25.4 ± 4.5** | **2.61 ± 0.7** | **33.4 ± 1.4** | Atoms x $10^9$ | 1.5 ± 0.2 |
| | *53.6 ± 9.8* | *5.60 ± 1.7* | *70.6 ± 6.6* | Atoms x $10^5/\mu m^2$ | |
| Early Blastocyst | **20.2 ± 3.9** | **1.85 ± 0.1** | **35.2 ± 0.8** | Atoms x $10^9$ | 2.3 ± 0.4 |
| | *47.0 ± 10.7* | *4.09 ± 0.4* | *78.2 ± 5.1* | Atoms x $10^5/\mu m^2$ | |
| Late Blastocyst | ***9.72 ± 0.8*** | ***2.40 ± 0.2*** | ***38.6 ± 1.7*** | Atoms x $10^9$ | 4.2 ± 0.3 |
| | *13.8 ± 1.7* | *3.29 ± 0.3* | *53.2 ± 4.2* | Atoms x $10^5/\mu m^2$ | |

Values in **bold** represent number of atoms x $10^9$ ± SEM. Values in *italics* represent the concentration of atoms x $10^5$ ± SEM. Zn:Fe is the ratio of total atoms of zinc to iron ± SEM. Fe=iron, Cu=copper, Zn=Zinc.

## References


BERNHARDT, M. L., KIM, A. M., O'HALLORAN, T. V. & WOODRUFF, T. K. 2011. Zinc requirement during meiosis I-meiosis II transition in mouse oocytes is independent of the MOS-MAPK pathway. *Biol Reprod,* 84**,** 526-36.

BERNHARDT, M. L., KONG, B. Y., KIM, A. M., O'HALLORAN, T. V. & WOODRUFF, T. K. 2012. A zinc-dependent mechanism regulates meiotic progression in mammalian oocytes. *Biol Reprod,* 86**,** 114.

CHEN, B., YU, P., CHAN, W. N., XIE, F., ZHANG, Y., LIANG, L., LEUNG, K. T., LO, K. W., YU, J., TSE, G. M. K., KANG, W. & TO, K. F. 2024. Cellular zinc metabolism and zinc signaling: from biological functions to diseases and therapeutic targets. *Signal Transduct Target Ther,* 9**,** 6.

CHEN, X., FANG, F., LIOU, Y.-C. & NG, H.-H. 2008. Zfp143 Regulates Nanog Through Modulation of Oct4 Binding. *Stem Cells,* 26**,** 2759-2767.

CHEN, X., ZHOU, Y., WU, D., SHU, C., WU, R., LI, S., HUANG, Q. & SHU, J. 2021. Iron overload compromises preimplantation mouse embryo development. *Reproductive Toxicology,* 105**,** 156-165.

CHEN, Y. Y., CHEN, S., OK, K., DUNCAN, F. E., O'HALLORAN, T. V. & WOODRUFF, T. K. 2023. Zinc dynamics regulate early ovarian follicle development. *J Biol Chem,* 299**,** 102731.

DENG, H., QIAO, X., XIE, T., FU, W., LI, H., ZHAO, Y., GUO, M., FENG, Y., CHEN, L., ZHAO, Y., MIAO, L., CHEN, C., SHEN, K. & WANG, X. 2021. SLC-30A9 is required for Zn(2+) homeostasis, Zn(2+) mobilization, and mitochondrial health. *Proc Natl Acad Sci U S A,* 118.

DUNCAN, F. E., QUE, E. L., ZHANG, N., FEINBERG, E. C., O'HALLORAN, T. V. & WOODRUFF, T. K. 2016. The zinc spark is an inorganic signature of human egg activation. *Sci Rep,* 6**,** 24737.

EIDE, D. J. 2006. Zinc transporters and the cellular trafficking of zinc. *Biochim Biophys Acta,* 1763**,** 711-22.

FIDALGO, M., SHEKAR, P. C., ANG, Y. S., FUJIWARA, Y., ORKIN, S. H. & WANG, J. 2011. Zfp281 functions as a transcriptional repressor for pluripotency of mouse embryonic stem cells. *Stem Cells,* 29**,** 1705-16.

FISHER, A. L., SANGKHAE, V., BALUSIKOVA, K., PALASKAS, N. J., GANZ, T. & NEMETH, E. 2021. Iron-dependent apoptosis causes embryotoxicity in inflamed and obese pregnancy. *Nat Commun,* 12**,** 4026.

GUZMAN, L., NUNEZ, D., LOPEZ, R., INOUE, N., PORTELLA, J., VIZCARRA, F., NORIEGA-PORTELLA, L., NORIEGA-HOCES, L. & MUNNE, S. 2019. The number of biopsied trophectoderm cells may affect pregnancy outcomes. *J Assist Reprod Genet,* 36**,** 145-151.

HOUGHTON, F. D. & LEESE, H. J. 2004. Metabolism and developmental competence of the preimplantation embryo. *Eur J Obstet Gynecol Reprod Biol,* 115 Suppl 1**,** S92-6.

HU, J., YANG, Z., WANG, J., YU, J., GUO, J., LIU, S., QIAN, C., SONG, L., WU, Y. & CHENG, J. 2016. Zinc Chloride Transiently Maintains Mouse Embryonic Stem Cell Pluripotency by Activating Stat3 Signaling. *PLoS One,* 11**,** e0148994.

JEDRUSIK, A. 2015. Making the first decision: lessons from the mouse. *Reprod Med Biol,* 14**,** 135-150.

KIM, A. M., BERNHARDT, M. L., KONG, B. Y., AHN, R. W., VOGT, S., WOODRUFF, T. K. & O'HALLORAN, T. V. 2011. Zinc sparks are triggered by fertilization and facilitate cell cycle resumption in mammalian eggs. *ACS Chem Biol,* 6**,** 716-23.

KIM, A. M., VOGT, S., O'HALLORAN, T. V. & WOODRUFF, T. K. 2010. Zinc availability regulates exit from meiosis in maturing mammalian oocytes. *Nat Chem Biol,* 6**,** 674-81.

KIM, J., CHU, J., SHEN, X., WANG, J. & ORKIN, S. H. 2008. An extended transcriptional network for pluripotency of embryonic stem cells. *Cell,* 132**,** 1049-61.

KONG, B. Y., BERNHARDT, M. L., KIM, A. M., O'HALLORAN, T. V. & WOODRUFF, T. K. 2012. Zinc maintains prophase I arrest in mouse oocytes through regulation of the MOS-MAPK pathway. *Biol Reprod,* 87**,** 11, 1-12.

KONG, B. Y., DUNCAN, F. E., QUE, E. L., XU, Y., VOGT, S., O'HALLORAN, T. V. & WOODRUFF, T. K. 2015. The inorganic anatomy of the mammalian preimplantation embryo and the requirement of zinc during the first mitotic divisions. *Dev Dyn,* 244**,** 935-47.

KONG, X., YANG, S., GONG, F., LU, C., ZHANG, S., LU, G. & LIN, G. 2016. The Relationship between Cell Number, Division Behavior and Developmental Potential of Cleavage Stage Human Embryos: A Time-Lapse Study. *PLoS One,* 11**,** e0153697.

KOWALCZYK, A., GBADAMOSI, O., KOLOR, K., SOSA, J., ANDRZEJCZUK, L., GIBSON, G., ST CROIX, C., CHIKINA, M., AIZENMAN, E., CLARK, N. & KISELYOV, K. 2021. Evolutionary rate covariation identifies SLC30A9 (ZnT9) as a mitochondrial zinc transporter. *Biochem J,* 478**,** 3205-3220.

LANE, M. & GARDNER, D. K. 1997. Differential regulation of mouse embryo development and viability by amino acids. *J Reprod Fertil,* 109**,** 153-64.

LIUZZI, J. P. & COUSINS, R. J. 2004. Mammalian zinc transporters. *Annu Rev Nutr,* 24**,** 151-72.

MAEMURA, M., TAKETSURU, H., NAKAJIMA, Y., SHAO, R., KAKIHARA, A., NOGAMI, J., OHKAWA, Y. & TSUKADA, Y. I. 2021. Totipotency of mouse zygotes extends to single blastomeres of embryos at the four-cell stage. *Sci Rep,* 11**,** 11167.

MITSUI, K., TOKUZAWA, Y., ITOH, H., SEGAWA, K., MURAKAMI, M., TAKAHASHI, K., MARUYAMA, M., MAEDA, M. & YAMANAKA, S. 2003. The homeoprotein Nanog is required for maintenance of pluripotency in mouse epiblast and ES cells. *Cell,* 113**,** 631-42.

MNATSAKANYAN, H., SABATER, I. S. R., SALMERON-SANCHEZ, M. & RICO, P. 2019. Zinc Maintains Embryonic Stem Cell Pluripotency and Multilineage Differentiation Potential via AKT Activation. *Front Cell Dev Biol,* 7**,** 180.

NG, S. W., NORWITZ, S. G. & NORWITZ, E. R. 2019. The Impact of Iron Overload and Ferroptosis on Reproductive Disorders in Humans: Implications for Preeclampsia. *Int J Mol Sci,* 20.

QUE, E. L., BLEHER, R., DUNCAN, F. E., KONG, B. Y., GLEBER, S. C., VOGT, S., CHEN, S., GARWIN, S. A., BAYER, A. R., DRAVID, V. P., WOODRUFF, T. K. & O'HALLORAN, T. V. 2015. Quantitative mapping of zinc fluxes in the mammalian egg reveals the origin of fertilization-induced zinc sparks. *Nat Chem,* 7**,** 130-9.

ROJAS, A., SCHACHTERLE, W., XU, S. M., MARTIN, F. & BLACK, B. L. 2010. Direct transcriptional regulation of Gata4 during early endoderm specification is controlled by FoxA2 binding to an intronic enhancer. *Dev Biol,* 346**,** 346-55.

SIEBER, M. H., THOMSEN, M. B. & SPRADLING, A. C. 2016. Electron Transport Chain Remodeling by GSK3 during Oogenesis Connects Nutrient State to Reproduction. *Cell,* 164**,** 420-32.

SUWINSKA, A., CZOLOWSKA, R., OZDZENSKI, W. & TARKOWSKI, A. K. 2008. Blastomeres of the mouse embryo lose totipotency after the fifth cleavage division: expression of Cdx2 and Oct4 and developmental potential of inner and outer blastomeres of 16- and 32-cell embryos. *Dev Biol,* 322**,** 133-44.

TAKAGISHI, T., HARA, T. & FUKADA, T. 2017. Recent Advances in the Role of SLC39A/ZIP Zinc Transporters In Vivo. *Int J Mol Sci,* 18.

TAKI, M., WOLFORD, J. L. & O'HALLORAN, T. V. 2004. Emission ratiometric imaging of intracellular zinc: design of a benzoxazole fluorescent sensor and its application in two-photon microscopy. *J Am Chem Soc,* 126**,** 712-3.

TIAN, X., ANTHONY, K., NEUBERGER, T. & DIAZ, F. J. 2014. Preconception zinc deficiency disrupts postimplantation fetal and placental development in mice. *Biol Reprod,* 90**,** 83.

URIU-ADAMS, J. Y. & KEEN, C. L. 2010. Zinc and reproduction: effects of zinc deficiency on prenatal and early postnatal development. *Birth Defects Res B Dev Reprod Toxicol,* 89**,** 313-25.

WANG, Z. X., TEH, C. H., CHAN, C. M., CHU, C., ROSSBACH, M., KUNARSO, G., ALLAPITCHAY, T. B., WONG, K. Y. & STANTON, L. W. 2008. The transcription factor Zfp281 controls embryonic stem cell pluripotency by direct activation and repression of target genes. *Stem Cells,* 26**,** 2791-9.

WU, G., GENTILE, L., FUCHIKAMI, T., SUTTER, J., PSATHAKI, K., ESTEVES, T. C., ARAUZO-BRAVO, M. J., ORTMEIER, C., VERBERK, G., ABE, K. & SCHOLER, H. R. 2010. Initiation of trophectoderm lineage specification in mouse embryos is independent of Cdx2. *Development,* 137**,** 4159-69.

XIE, F., TIMME, K. A. & WOOD, J. R. 2018. Using Single Molecule mRNA Fluorescent in Situ Hybridization (RNA-FISH) to Quantify mRNAs in Individual Murine Oocytes and Embryos. *Sci Rep,* 8**,** 7930.

ZERNICKA-GOETZ, M., MORRIS, S. A. & BRUCE, A. W. 2009. Making a firm decision: multifaceted regulation of cell fate in the early mouse embryo. *Nat Rev Genet,* 10**,** 467-77.

ZIGO, M., KERNS, K., SEN, S., ESSIEN, C., OKO, R., XU, D. & SUTOVSKY, P. 2022. Zinc is a master-regulator of sperm function associated with binding, motility, and metabolic modulation during porcine sperm capacitation. *Communications Biology,* 5**,** 538.

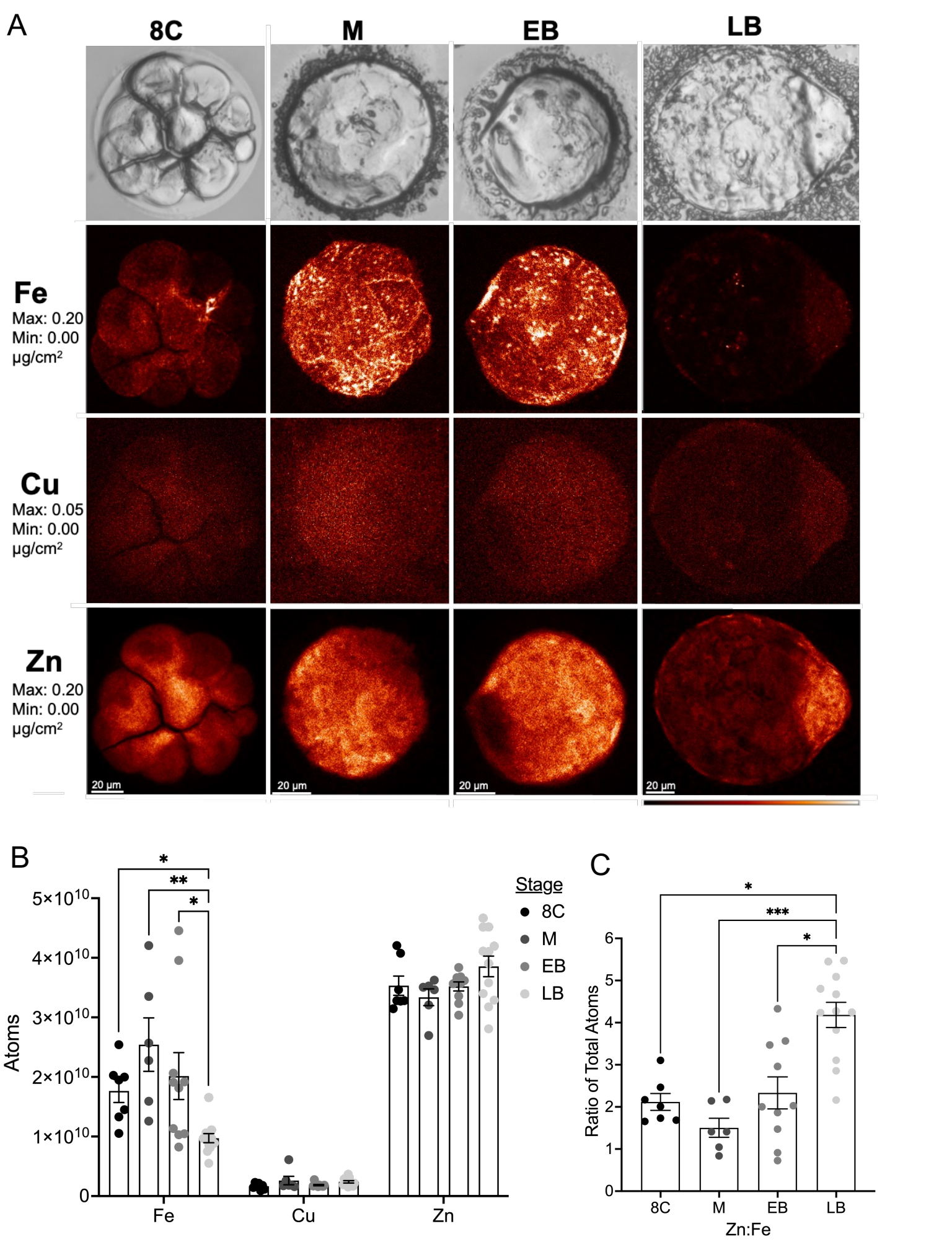
A
8C
M
EB
LB
Fe
Max: 0.20
Min: 0.00
µg/cm²
Cu
Max: 0.05
Min: 0.00
µg/cm²
Zn
Max: 0.20
Min: 0.00
µg/cm²
20 µm
20 µm
20 µm
20 µm
B
Atoms
5×10¹⁰
4×10¹⁰
3×10¹⁰
2×10¹⁰
1×10¹⁰
0
Fe
Cu
Zn
Stage
8C
M
EB
LB
C
Ratio of Total Atoms
0
1
2
3
4
5
6
8C
M
EB
LB
Zn:Fe

Figure 1

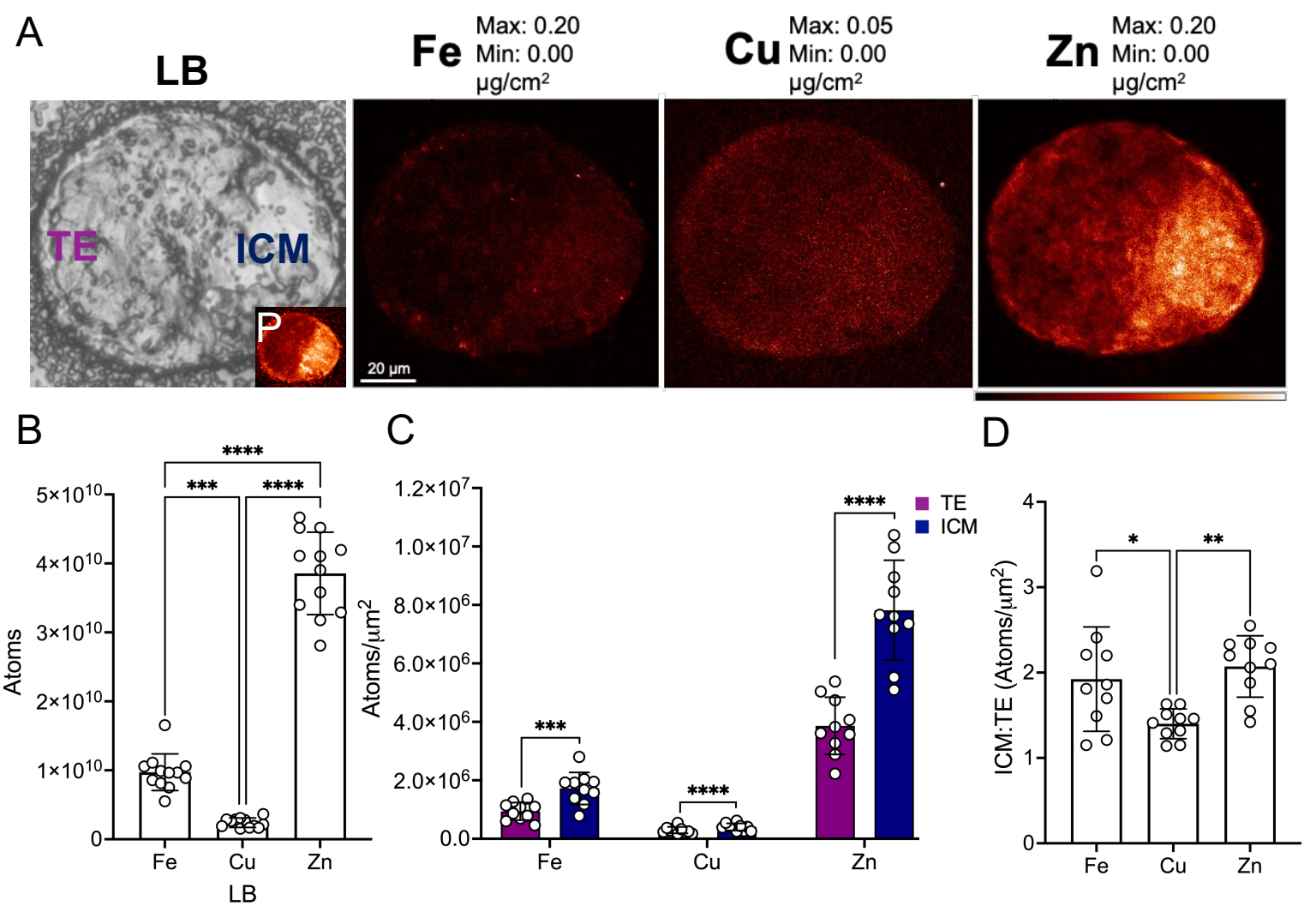
A
LB
TE
ICM
P
Fe
Max: 0.20
Min: 0.00
µg/cm²
Cu
Max: 0.05
Min: 0.00
µg/cm²
Zn
Max: 0.20
Min: 0.00
µg/cm²
20 µm
B
Atoms
5×10¹⁰
4×10¹⁰
3×10¹⁰
2×10¹⁰
1×10¹⁰
0
****
***
****
Fe
Cu
Zn
LB
C
Atoms/µm²
1.2×10⁷
1.0×10⁷
8.0×10⁶
6.0×10⁶
4.0×10⁶
2.0×10⁶
0.0
TE
ICM
***
****
****
Fe
Cu
Zn
D
ICM:TE (Atoms/µm²)
4
3
2
1
0
*
**
Fe
Cu
Zn

Figure 2

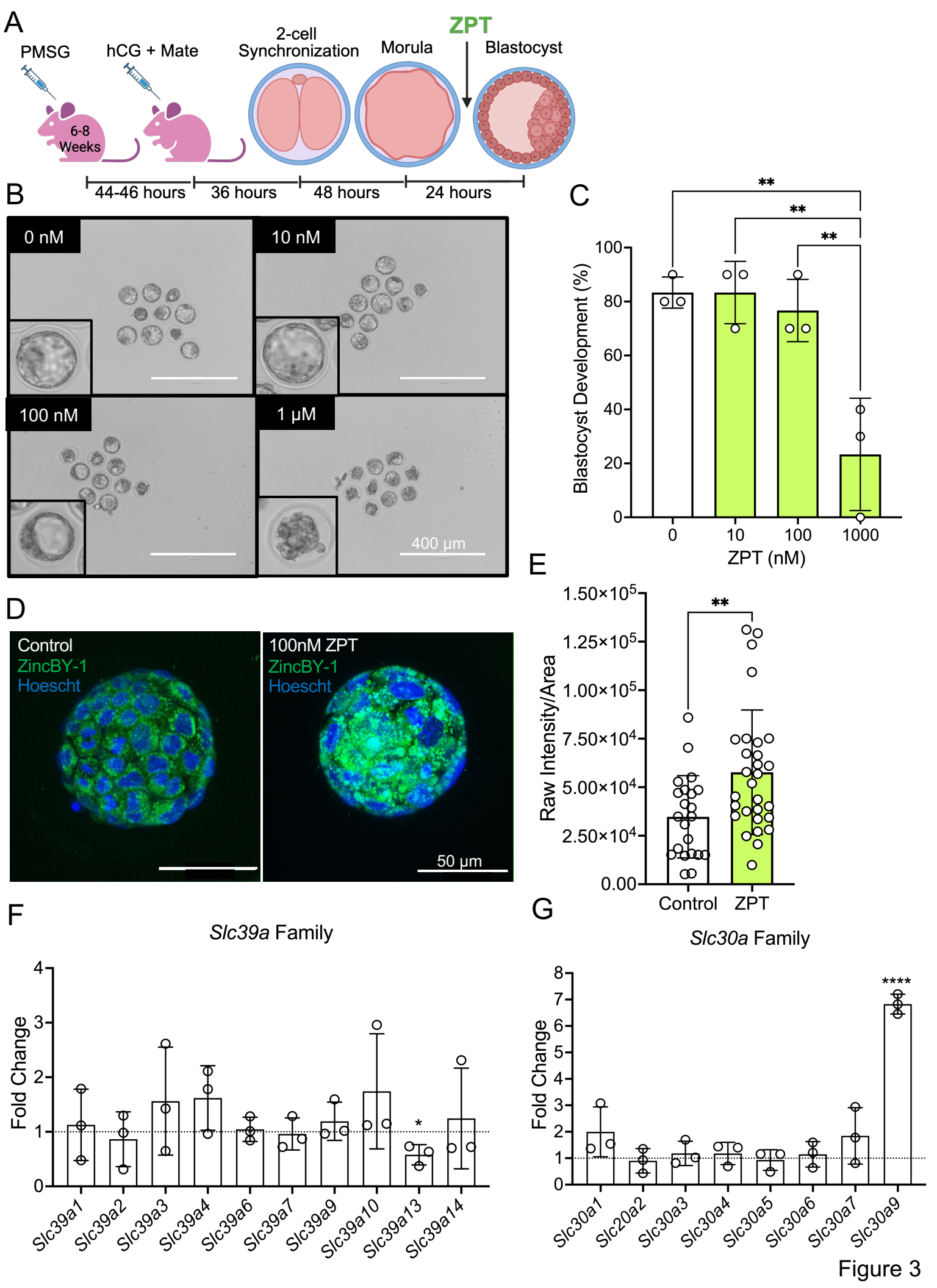
A
PMSG
hCG + Mate
6-8 Weeks
2-cell Synchronization
Morula
ZPT
Blastocyst
44-46 hours
36 hours
48 hours
24 hours
B
0 nM
10 nM
100 nM
1 µM
400 µm
C
Blastocyst Development (%)
ZPT (nM)
0
10
100
1000
D
Control
ZincBY-1
Hoescht
100nM ZPT
ZincBY-1
Hoescht
50 µm
E
Raw Intensity/Area
Control
ZPT
F
Slc39a Family
Fold Change
Slc39a1
Slc39a2
Slc39a3
Slc39a4
Slc39a6
Slc39a7
Slc39a9
Slc39a10
Slc39a13
Slc39a14
G
Slc30a Family
Fold Change
Slc30a1
Slc20a2
Slc30a3
Slc30a4
Slc30a5
Slc30a6
Slc30a7
Slc30a9

Figure 3

A

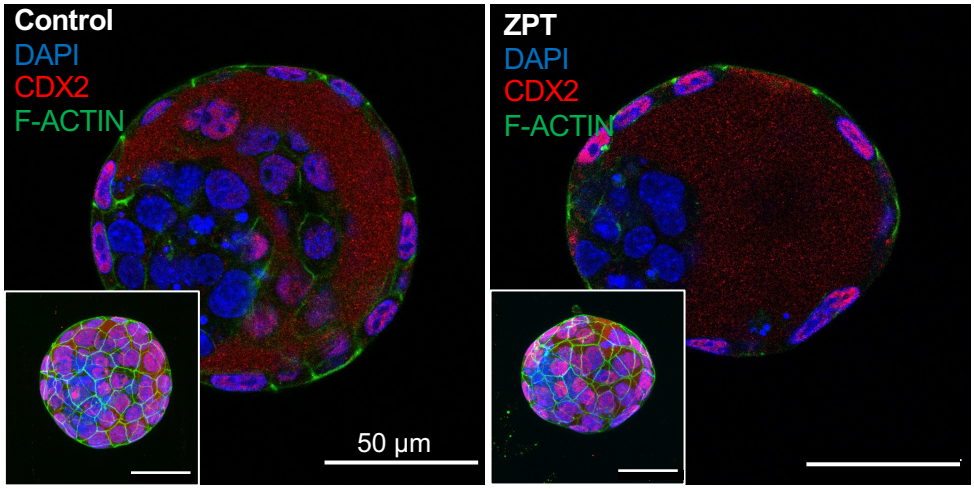


B

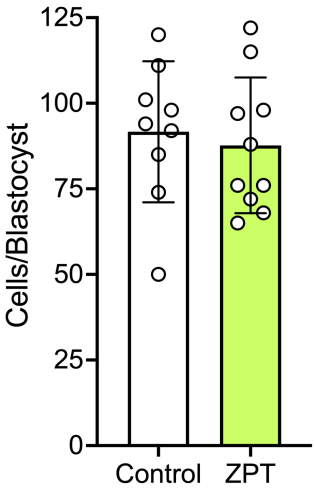


C

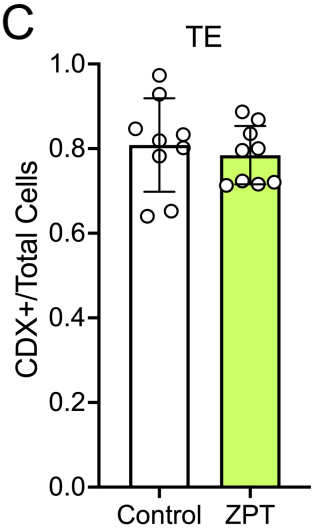


D

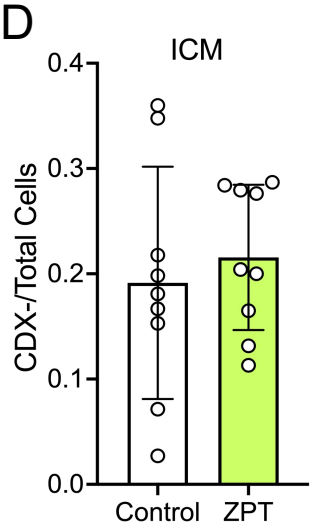


E

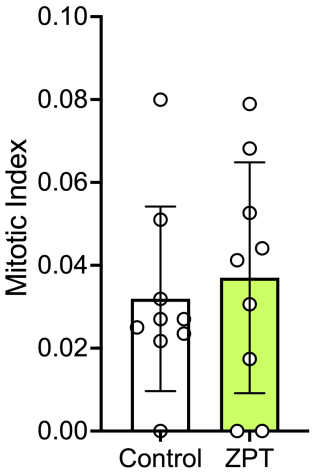


F

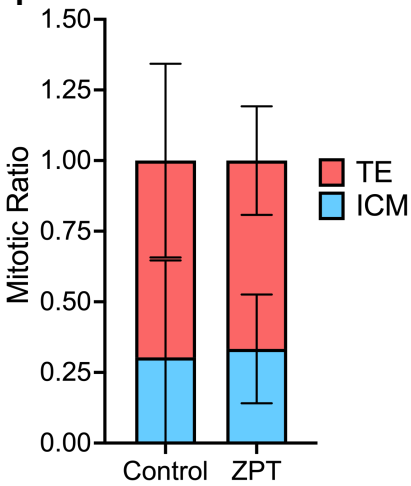


Figure 4

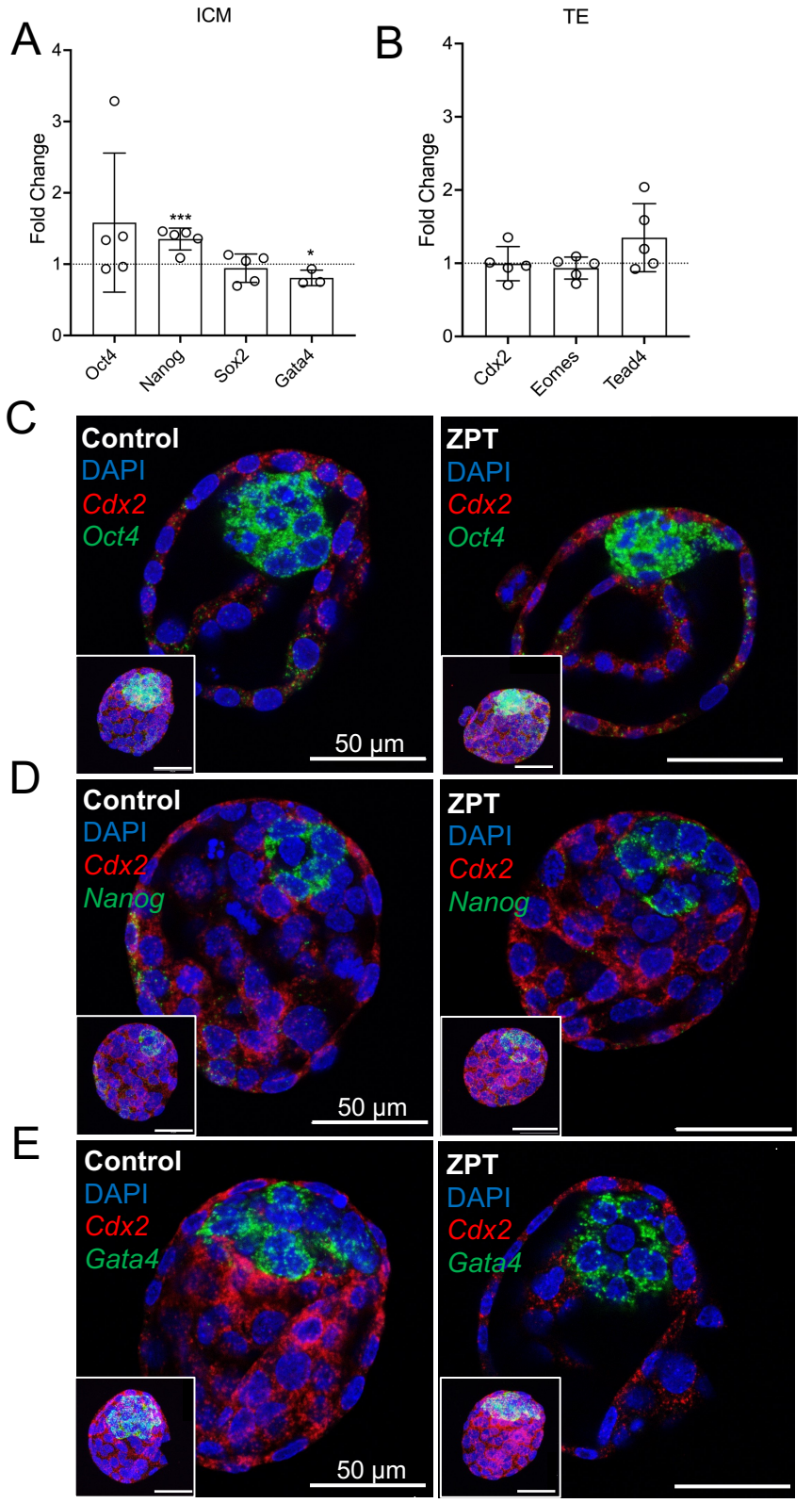
A
ICM
Fold Change
Oct4
Nanog
Sox2
Gata4
B
TE
Fold Change
Cdx2
Eomes
Tead4
C
Control
DAPI
Cdx2
Oct4
ZPT
DAPI
Cdx2
Oct4
50 µm
D
Control
DAPI
Cdx2
Nanog
ZPT
DAPI
Cdx2
Nanog
50 µm
E
Control
DAPI
Cdx2
Gata4
ZPT
DAPI
Cdx2
Gata4
50 µm

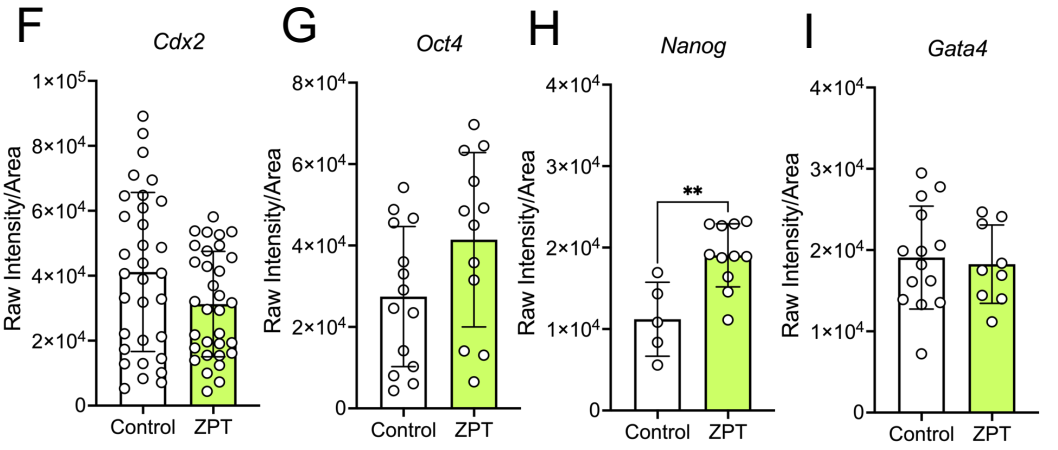
F
Cdx2
Raw Intensity/Area
Control
ZPT
G
Oct4
Raw Intensity/Area
Control
ZPT
H
Nanog
Raw Intensity/Area
Control
ZPT
I
Gata4
Raw Intensity/Area
Control
ZPT

Figure 5